Single-Molecule Magnets

Substrate-Independent Magnetic Bistability in Monolayers of the Single-Molecule Magnet Dy₂ScN@C₈₀ on Metals and Insulators

Denis S. Krylov[+],* Sebastian Schimmel[+], Vasilii Dubrovin[+], Fupin Liu, T. T. Nhung Nguyen, Lukas Spree, Chia-Hsiang Chen, Georgios Velkos, Claudiu Bulbucan, Rasmus Westerström, Michał Studniarek, Jan Dreiser, Christian Hess, Bernd Büchner, Stanislav M. Avdoshenko,* and Alexey A. Popov*

Abstract: Magnetic hysteresis is demonstrated for monolayers of the single-molecule magnet (SMM) Dy₂ScN@C₈₀ deposited on Au(111), Ag(100), and MgO | Ag(100) surfaces by vacuum sublimation. The topography and electronic structure of Dy₂ScN@C₈₀ adsorbed on Au(111) were studied by STM. X-ray magnetic CD studies show that the Dy₂ScN@C₈₀ monolayers exhibit similarly broad magnetic hysteresis independent on the substrate used, but the orientation of the Dy₂ScN cluster depends strongly on the surface. DFT calculations show that the extent of the electronic interaction of the fullerene molecules with the surface is increasing dramatically from MgO to Au(111) and Ag(100). However, the charge redistribution at the fullerene-surface interface is fully absorbed by the carbon cage, leaving the state of the endohedral cluster intact. This Faraday cage effect of the fullerene preserves the magnetic bistability of fullerene-SMMs on conducting substrates and facilitates their application in molecular spintronics.

Introduction

Single-molecule magnets (SMMs) are molecular materials exhibiting magnetic bistability and slow relaxation of magnetization.[1] Since these properties should be preserved even for single molecules, the prospects of SMMs in information storage and spintronics[2] have been pushing the field toward developing new molecules with better SMM performance and higher operating temperatures.[3] So far, the vast majority of the studies of SMMs have been performed for their powders and crystals. At the same time, realization of the true advantages of SMMs over bulk magnetic materials require the scaling down to 2D, 1D, and eventually a single-molecule

level. Investigation of the magnetic properties of monolayers is thus the next logical step after the bulk SMM behavior is established.[4] However, formation of monolayers requires certain chemical and/or thermal stability, which many SMMs do not have, whereas surface techniques for the study of the sample morphology or magnetism are rather complicated. As a result, the SMMs, whose magnetic properties have been studied on surfaces, are very rare in comparison to hundreds of known SMM compounds. The scaling down to monolayer level also raises a question of the substrate influence on the SMM properties of adsorbed molecules. In particular, interaction with conducting electrons is believed to be deteriorating for the SMM behavior. So far, magnetic hysteresis on conducting substrates was demonstrated only for three types of SMMs: LnPc₂ (Ln = Tb, Dy),[5] Fe₄,[6] and metallofullerenes Dy₁₍₂₎Sc₂₍₁₎N@C₈₀.[7]

Endohedral metallofullerenes[8] form a special class of SMMs in which lanthanides are encapsulated within the carbon cage.[9] This allows stabilization of unusual lanthanide clusters with strong single-ion magnetic anisotropy[10] or giant exchange coupling.[11] Furthermore, high thermal stability of fullerenes enables formation of monolayers by sublimation.[12] The first study of the surface magnetism of the fullerene-SMM monolayer was performed by X-ray magnetic circular dichroism (XMCD) technique for Dy₂ScN@C₈₀ on Rh(111) and indeed revealed a magnetic bistability.[7a] However, magnetic hysteresis of the monolayer was considerably narrower than for a multilayer sample. A broader hysteresis than on Rh(111) was observed for Dy₂ScN@C₈₀ on *h*-BN | Rh(111).[7b] Here we demonstrate that the SMM properties of Dy₂ScN@C₈₀ monolayers on Au(111) and Ag(100), as well on

---

[*] Dr. D. S. Krylov,[+] S. Schimmel,[+] V. Dubrovin,[+] Dr. F. Liu,
T. T. N. Nguyen, L. Spree, Prof. C.-H. Chen, G. Velkos, Dr. C. Hess,
Prof. Dr. B. Büchner, Dr. S. M. Avdoshenko, Dr. A. A. Popov
Leibniz Institute for Solid State and Materials Research
Helmholtzstraße 20, 01069 Dresden (Germany)
E-mail: dskrylov@gmail.com
s.avdoshenko@ifw-dresden.de
a.popov@ifw-dresden.de

Dr. D. S. Krylov[+]
Center for Quantum Nanoscience, Institute for Basic Science (IBS)
Seoul (Republic of Korea)

Prof. C.-H. Chen
Department of Medicinal and Applied Chemistry
Kaohsiung Medical University
Kaohsiung 807 (Taiwan)

C. Bulbucan, Dr. R. Westerström
The division of synchrotron radiation research, Lund University
22100 Lund (Sweden)

Dr. M. Studniarek, Dr. J. Dreiser
Swiss Light Source, Paul Scherrer Institute
5232 Villigen PSI (Switzerland)

[+] These authors contributed equally to this work.

Supporting information and the ORCID identification number(s) for the author(s) of this article can be found under:
https://doi.org/10.1002/anie.201913955.

a thin film of insulator MgO grown on Ag(100), do not depend on the substrate, which highlights the robustness of fullerene SMMs and the protective function of the carbon cage.

Results and Discussion

The molecule of $Dy_2ScN@C_{80}$ is built from an icosahedral carbon cage C_{80}-I_h, which encapsulates a planar metal nitride cluster Dy_2ScN (Figure 1a). The nitride ion N^{3-} is located in
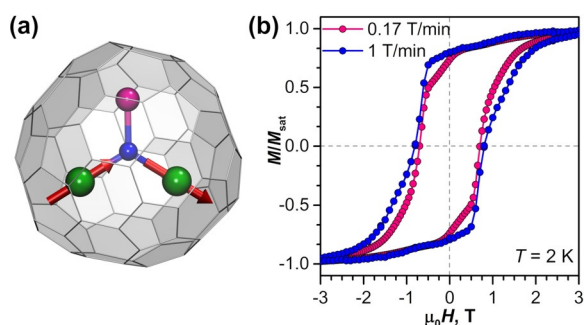

Figure 1. a) Molecular structure of $Dy_2ScN@C_{80}$ (Dy green, N blue, Sc magenta; magnetic moments of Dy ions are visualized as red arrows). b) Magnetic hysteresis measured for the powder sample of $Dy_2ScN@C_{80}$ by SQUID magnetometry at $T = 2$ K with magnetic field sweep rates of 0.17 and 1 T min^{-1}.

the center of a triangle formed by metal ions in their formal oxidation state of 3+. Dy−N bond lengths in $Dy_2ScN@C_{80}$ are shorter than 2.1 Å,[10b] which results in a strong uniaxial ligand field imposed by the nitride onto Dy^{3+} ions.[10b,13] The magnetic ground state of each Dy^{3+} ion is a Kramers doublet with $m_J = \pm 15/2$ and a quantization axis aligned along the corresponding Dy−N bond. Very large ligand-field splitting ensures that single-ion magnetic moments are locked to the Dy−N bonds up to high temperature. The intramolecular interactions between magnetic moments of Dy ions are predominantly ferromagnetic (Figure 1a), and the state with anti-parallel alignment of magnetic moment is higher in energy by 0.8 meV (10 K).[10b,14] $Dy_2ScN@C_{80}$ is a single-molecule magnet with a blocking temperature of magnetization near 8 K and a 100 s blocking temperature of 5 K.[10b] At 2 K, the powder sample of $Dy_2ScN@C_{80}$ shows magnetic hysteresis with a coercive field of 0.7–0.8 T (Figure 1b).

To ensure the suitability of the evaporated thin films of $Dy_2ScN@C_{80}$ for the studies of magnetic properties by XMCD technique, deposition of the fullerene onto Au(111) substrate and characterization of the monolayer properties by scanning tunneling microscopy (STM) were first performed. The molecules were deposited under ultra-high-vacuum conditions ($p \leq 10^{-9}$ mbar) via organic molecular beam epitaxy using a home build evaporator. Typical evaporation conditions were 20 minutes at 450–460 °C. The substrate was kept at room temperature during deposition, and STM studies were also performed at room temperature using Omicron VT-STM/AFM microscope.

STM measurements revealed that at these evaporation conditions the surface of the substrate is covered with ca. 0.5 ML of fullerene molecules (Supporting Information, Figure S1). The endohedral fullerenes diffuse across the terraces of Au(111) and self-assemble into closed monolayer islands of several 10×10 nm^2 anchored to the edges of the substrate step (Figure 2a). As already observed for other $M_3N@C_{80}$ fullerenes on Au(111),[12a–c] $Dy_2ScN@C_{80}$ molecules are organized in a hexagonal close-packed (hcp) structure with a lattice parameter of 1.15 ± 0.05 nm (Figure 2b). Fourier transformation of the topographic image gives Bragg peak positions proving a three-fold symmetric periodic structure (Figure 2b). On the bare part of the Au(111) substrate, the herringbone reconstruction typical for a clean Au(111) surface is observed (Figure 1a). The reconstruction double stripes also appear on and across the monolayer islands (Figure 2a,b), but the inter-stripe distance and their course varies from that of unperturbed Au(111): The density of reconstruction stripes under the fullerene layer is reduced, whereas the Au(111) fcc-like terminated areas in between the double stripes become wider in comparison to the pristine herringbone pattern. Thus, the formation of quasi-epitaxial 4×4 superstructure of fullerenes on Au(111) fcc sites is enhanced and consequently the interface energy is reduced.[12a,c,15] The facts that the fullerenes show a sufficiently high mobility at RT to form monolayer islands and that the herringbone reconstruction is not fully lifted at the interface imply a comparably weak interaction of $Dy_2ScN@C_{80}$ molecules with the Au(111) surface.

The electronic structure of $Dy_2ScN@C_{80}$ on Au(111) was studied by scanning tunneling spectroscopy (STS). The spectra acquired in the field of view presented in Figure 2b showed four somewhat different patterns (Figure 2c) occurring with almost equal abundance. Presumably, they are caused by different tip position over fullerenes and by different adsorption geometries of the $Dy_2ScN@C_{80}$ molecules on the Au(111) surface.[16] The noticeable difference between the splitting patterns demonstrates that the fullerene–fullerene and fullerene–substrate interactions are not negligible.[17] Each spectrum type exhibits a well-defined gap and distinct peaks corresponding to the occupied and unoccupied states of the fullerene molecule. DFT calculations show (see discussion below and in Supporting Information), that the density of fullerene states is rather high, and each peak in STS spectra corresponds to several fullerene orbitals. The HOMO-derived state overlaps with other lower-energy occupied states and form a peak at −(0.9–1) V. For the fullerene LUMO, DFT calculations predict a stand-alone peak at the energy near +0.6 V above Fermi level, whereas other unoccupied orbitals are densely packed in the energy range above +1 V. Calculations also show that depending on the orientation of the endohedral cluster inside the fullerene versus the substrate, the orbital energies may vary within the range of 0.2–0.3 eV. Based on these predictions, we tentatively suggest that the LUMO-derived states may corresponds to the features marked by asterisks in Figure 2c. In the average spectrum of the whole studied area (Figure 2d), these fine features are smeared out, leading to an effective energy gap of
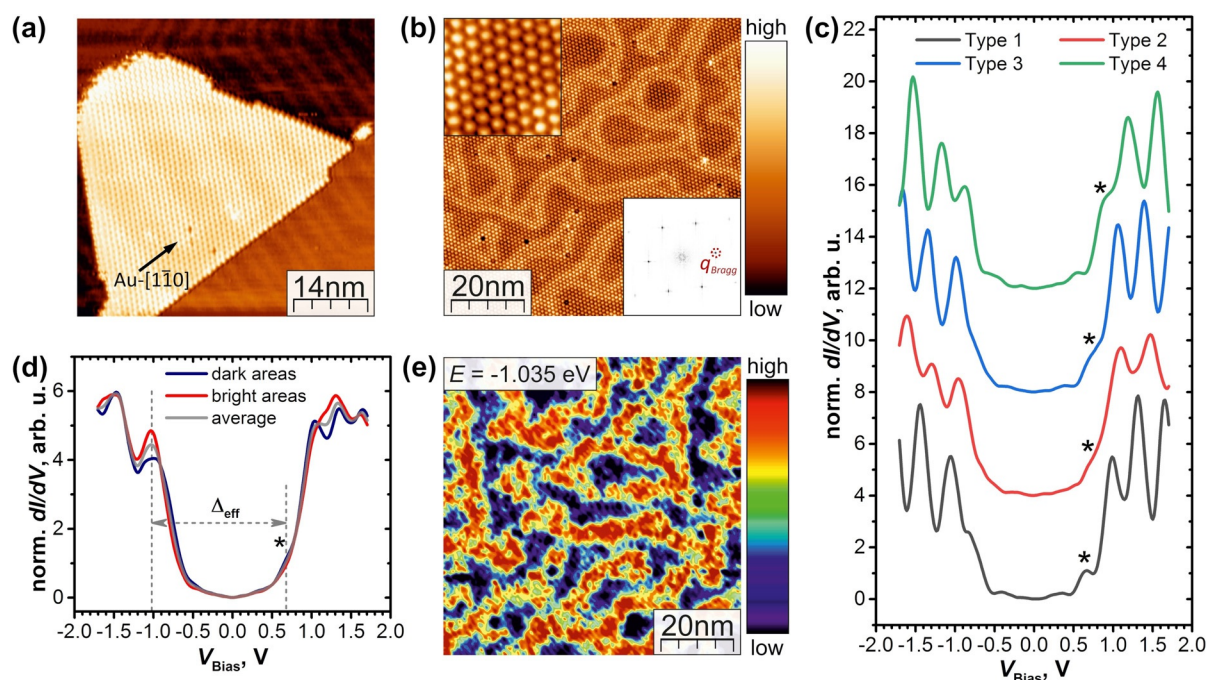
Figure 2. a) Constant current topography image of an hcp monolayer island of $Dy_2ScN@C_{80}$ on Au(111) surface anchored to the Au(111) step edge ($V_{Bias} = 2$ V; $I_{Set} = 200$ pA); the arrow indicates the fullerenes closed packed direction coinciding with the Au-[110] direction; the features of the reconstruction are altered at the interface. b) The field of view of the constant current topography image of the $Dy_2ScN@C_{80}$ monolayer on Au(111) ($V_{Bias} = 1.5$ V; $I_{Set} = 600$ pA) in which the electronic structure was investigated; the left upper inset shows the hcp arrangement of the single fullerenes and in the lower right inset the FFT of the image is presented. c) Four types of STS spectra measured for $Dy_2ScN@C_{80}$ monolayer on Au(111); asterisks mark features tentatively assigned to the fullerene LUMO. d) The average STS spectrum over the area shown in (b), revealing an effective gap of $\Delta_{eff} = 1.7 \pm 0.1$ eV (gray curve) and the spectra averaged over two areas in (e) (red and blue curves). e) The $dln(I)/dln(V)$-map measured at the HOMO level energy of $E = -1.035$ eV showing the spatial variations of the electronic structure attributed to the altered herringbone reconstruction at the interface to the fullerene monolayer. Average spectra of the regions in between the stripes (dark blue in (e)) and on the stripes (yellow/red in (e)) are presented in (d).

$\Delta_{eff} = 1.7 \pm 0.1$ eV if the shoulder at $+0.7$ V is assigned to the LUMO or $\Delta_{eff} = 2.05 \pm 0.1$ eV if only peak maxima are used.

The normalized differential conductance map (Figure 2e) measured in the field of view shown in Figure 2b illustrates that additional spatial variations of the electronic structure of the monolayer emerge from the formation of the Au(111) reconstruction at the interface with $Dy_2ScN@C_{80}$. At the HOMO energy of -1.035 eV below the Fermi level, regions of supposed Au(111) fcc-like termination in between the topographically brighter double stripes in Figure 2b are imaged in dark blue (Figure 2e). They reveal a reduced local density of states in comparison to double stripe regions of the Au(111) hcp-like and ridge-like terminations, which correspond to the yellow–red region in Figure 2e. This effect can be also seen as the difference of the HOMO-derived peak heights in the STS spectra averaged over corresponding areas (Figure 2d). Obviously, the adsorption sites of $Dy_2ScN@C_{80}$ molecules on Au(111) vary following the altered reconstruction from quasi-epitaxial regions (in between the double stripes) to incommensurate double stripe areas, which affects the local electronic structure of the fullerene | metal interface.[18] Note that the four types of STS spectra shown in Figure 2c are found for both dark blue and bright red regions in Figure 2e (Supporting Information, Figure S2).

The magnetic properties of $Dy_2ScN@C_{80}$ monolayers were studied by Dy-$M_{4,5}$ XMCD at the X-Treme beam line at the

Swiss Light Source, Paul Scherrer Institut.[19] The magnetic field was kept parallel to the X-ray beam in all measurements. The thin film of MgO (10–11 ML) on Ag(100) was grown by sublimation of Mg in O_2 atmosphere (10^{-6} mbar) while keeping the substrate at 645 K. $Dy_2ScN@C_{80}$ evaporation conditions onto the Au(111) substrate were adopted from the ex situ studies described above. In situ characterization by STM confirmed formation of similar monolayer islands (Supporting Information, Figure S3). The same evaporation conditions were then used for the growth on Ag(100) and MgO | Ag(100), for which in situ STM characterization was not possible during the beamtime. The coverage of the Ag(100) and MgO | Ag(100) substrates by $Dy_2ScN@C_{80}$ was lower than for Au(111) (as estimated from XAS intensity), which ensures that all XMCD measurements were performed in the submonolayer regime. At the base temperature of the cryostat the temperature at the sample was near 2 K for the Au(111) crystal as estimated from separate measurements of Er(trensal)[20] powder (Supporting Information, Figure S4). For Ag(100) and MgO | Ag(100) substrates the temperature may be slightly higher (up to ca 2.5 K).

Dy-M_5 XAS and XMCD spectra of $Dy_2ScN@C_{80}$ submonolayers measured at $T \approx 2$ K in the magnetic field of 6.5 T are shown in Figure 3. The measurements at a different incidence of X-rays and magnetic field show a noticeable difference between the substrates. On Au(111), the XMCD
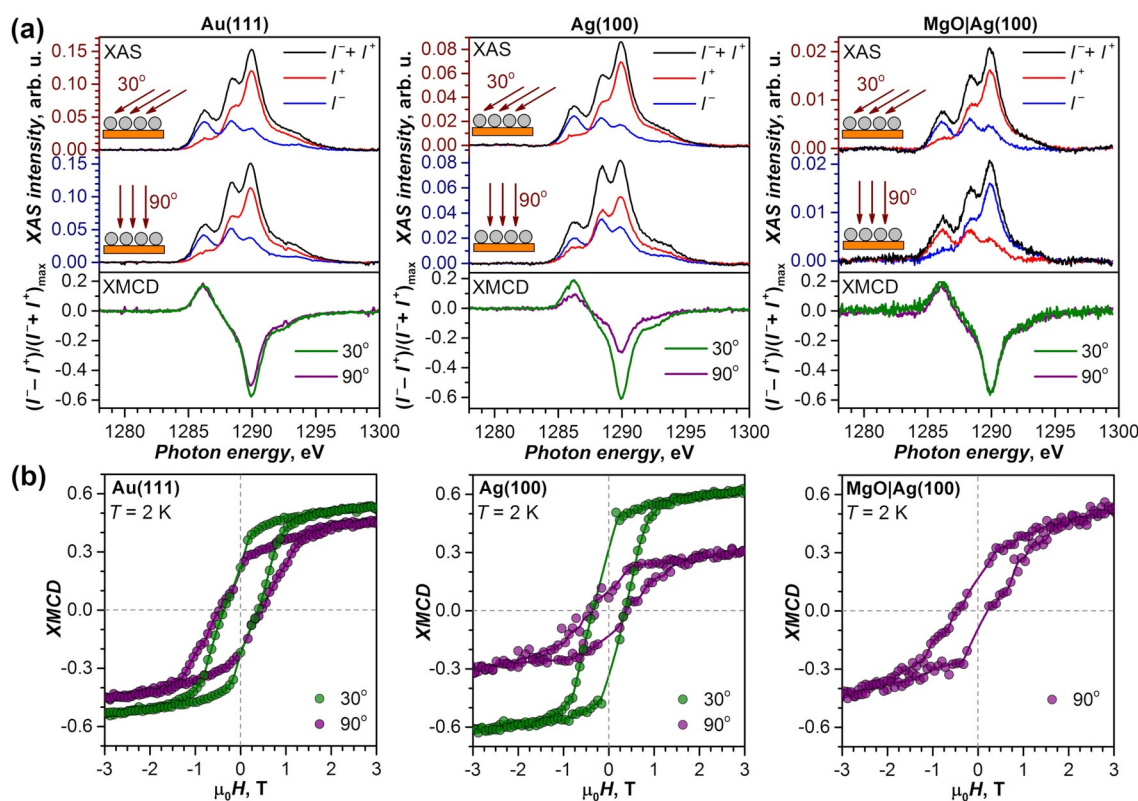
Figure 3. a) XAS and XMCD spectra of $Dy_2ScN@C_{80}$ sub-monolayers on Au(111), Ag(100), and MgO|Ag(100) measured at 30° and 90° orientation of the X-ray and magnetic field versus the surface; $T \approx 2$ K, $H = 6.5$ T, only the Dy-M_5 edge is shown (see the Supporting Information for the whole Dy-$M_{5,4}$ range). X-ray polarizations are denoted at I^+ and I^-, non-polarized XAS is a sum of I^+ and I^-, and XMCD is their difference normalized to the XAS maximum. b) Magnetic hysteresis of $Dy_2ScN@C_{80}$ on Au(111), Ag(100), and MgO|Ag(100) measured by XMCD technique at $T \approx 2$ K, sweep rate 2 Tmin^{-1}; dots are experimental values, and lines are added to guide the eye. For Au(111) and Ag(100), hysteresis measurements are shown for two angles of the X-ray and magnetic field versus the surface.

signal of $Dy_2ScN@C_{80}$ is slightly stronger in the grazing (30°) than in the normal (90°) incidence. On Ag(100), the difference between the two orientations is enhanced, with much stronger XMCD response at the grazing incidence. Finally, no difference can be seen between the spectra measured at 30° and 90° on the MgO|Ag(100) substrate. These results are further corroborated by the angular dependence of XMCD asymmetry (Figure 4), which is almost isotropic for Au(111) with a slight increase at smaller angles, isotropic for MgO|
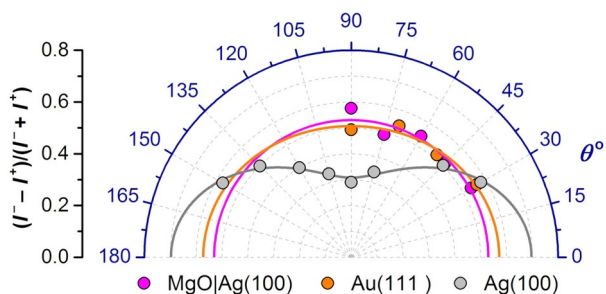

Figure 4. Angular dependence of XMCD asymmetry for the $Dy_2ScN@C_{80}$ submonolayer on Au(111), Ag(100), and MgO|Ag(100) measured at 1290 eV at $T \approx 2$ K. θ is the angle between X-ray beam/magnetic field and the surface. Dots are experimental values, lines are fits with the function $C_1 \cos^2(\theta) + C_2$.

Ag(100) within the experimental uncertainty, but strongly anisotropic for the Ag(100) substrate.

As magnetic moments of Dy ions are strongly anisotropic and are locked to the direction of the Dy−N bonds (Figure 1a), the angular dependence of XMCD essentially provides information on the orientation of the Dy_2ScN clusters in the monolayers. The isotropic behavior of the XMCD signal on Au(111) and MgO|Ag(100) shows that the Dy_2ScN cluster is randomly oriented in the $Dy_2ScN@C_{80}$ monolayers on these substrates. On the other hand, the anisotropy of the XMCD in the $Dy_2ScN@C_{80}$ monolayer on Ag(100) indicates that the endohedral cluster preferentially adopts a parallel orientation with respect to the surface. Parallel alignment of Dy_2ScN was also observed for the $Dy_2ScN@C_{80}$ monolayer on Rh(111).[7a]

The magnetic moment of Dy^{3+} ions in $Dy_2ScN@C_{80}$ can be estimated using XMCD sum rules.[21] For $Dy_2ScN@C_{80}$ on Au(111), the sum rule analysis gives the moment of 5.4 ± 0.5 μ_B per Dy^{3+} ion at 90° and 6.1 ± 0.5 μ_B at 30°. On Ag(100), the moment increases from 2.9 ± 0.5 μ_B at 90° to 5.7 ± 0.5 μ_B at 30°. These values are significantly smaller than 10 μ_B, the ground-state magnetic moment of Dy^{3+} ion in the axial ligand field. However, when magnetic moments are anisotropic, the measured moment corresponds to the projection of the magnetic field onto the easy axis. As a result, in powder

samples of $Dy_2ScN@C_{80}$ with disordered Dy_2ScN clusters, the apparent magnetic moment of Dy^{3+} ions is reduced to 5 μ_B.[14] The magnetic moments of Dy^{3+} ions in $Dy_2ScN@C_{80}$ on the Au(111) substrate are thus close to the value expected for the disordered cluster, which agrees with the lack of the angular dependence of the XMCD. For $Dy_2ScN@C_{80}$ on the Ag(100) substrates, the small magnetization perpendicular to the surface agrees well with the preferential in-plane alignment of the endohedral cluster.

The XMCD signal at the Dy-M_5 edge was used to study magnetization curves of $Dy_2ScN@C_{80}$ monolayers. Magnetic hysteresis with a coercive field of ca 0.4 T is observed for $Dy_2ScN@C_{80}$ monolayers on all three substrates near 2 K (Figure 2b). When temperature is increased to about 6 K, the hysteresis is not observed any more (Supporting Information, Figure S7). The asymmetric orientation of the Dy_2ScN cluster is also reflected in magnetization curves measured at 30° and 90° on Au(111) and Ag(100) substrates (Figure 3b). This width of the 2 K hysteresis is twice smaller than for the powder sample measured by SQUID magnetometry at a comparable sweep rate (Figure 1b). A possible reason is the X-ray-induced demagnetization.[22] Besides, changing polarity of the magnet during the field ramp takes 30 seconds, which also reduces the observed coercive field. Taking this into account, we conclude that there is no dramatic deterioration of the hysteretic behavior of $Dy_2ScN@C_{80}$ monolayers when compared to the bulk samples. Apparently, the fullerene cage provides sufficient protection for the endohedral magnetic cluster from the demagnetizing influence of metallic substrates. Earlier it was found that a thin layer of MgO dramatically increases the hysteresis of a $TbPc_2$ monolayer[5c,23] and boosts the temperature of the magnetic bistability of Ho atoms up to 30 K.[24] Recently, some of us showed that the improved SMM properties on MgO substrate are caused by its low phonon density of states, which leads to the dramatic reduction of the relaxation of magnetization via the Raman mechanism.[23] Apparently, this is not the relaxation rate-limiting factor for $Dy_2ScN@C_{80}$, and the use of the MgO layer does not lead to a noticeable improvement of the surface SMM behavior in comparison to metallic substrates. Thus, we conclude that the substrate plays an important role in the structural ordering of endohedral cluster, but has no strong influence on the SMM properties of adsorbed metallofullerenes. Therefore, the SMM performance of $Dy_2ScN@C_{80}$ monolayers is not limited by the interactions with the substrate.

For a deeper insight into the fullerene-substrate interactions, DFT calculations of the $Dy_2ScN@C_{80}$ molecule placed on Au(111), Ag(100), and MgO surfaces were performed at the PBE-D level with PAW 4f-in-core potentials using the VASP 5.0 code.[25] As the Dy_2ScN cluster may adopt different orientations inside the carbon cage, it is important to have a comprehensive sampling of possible structural configurations. Using recently proposed Fibonacci sphere sampling,[26] 120 initial configurations with different orientations of the Dy_2ScN cluster were generated for a fullerene molecule on each substrate, and their structures were optimized. For an isolated $Dy_2ScN@C_{80}$ molecule this approach gave only three unique conformers with the relative energies of 0, 41, and

47 meV. But a substantially different situation is found for $Dy_2ScN@C_{80}$ molecule on a substrate (Figure 5a,b). Calculations did not reveal any particularly stable conformation but rather predicted a multitude of conformers, which are likely to coexist under experimental conditions within a certain energy cut-off. The energies of the on-surface optimized conformers are spread in the range of 300 meV for Au(111) and Ag(100) substrates and 170 meV for the MgO substrate. It should be emphasized that these conformer distributions are predicted for a single $Dy_2ScN@C_{80}$ molecule in the absence of other fullerene neighbors. Due to the incommensurate lattice parameters of the substrates and the fullerene layer, calculations of the $Dy_2ScN@C_{80}$ monolayer are not feasible at this time. It can be anticipated that the intermolecular interactions should also affect the energetics of the cluster orientations and electronic properties,[26] but the influence of the metallic substrate is expected to be considerably stronger.

For $Dy_2ScN@C_{80}$ on Au(111) and Ag(100), the lowest-energy conformers are grouped at $\theta = 5–30°$, which corresponds to nearly parallel orientations of the cluster to the substrate. These results agree well with the observation of the in-plane ordering of the Dy_2ScN cluster on the Ag(100) surface, but do not fully capture the experimental finding of the weaker ordering effect on the Au(111) substrate. Presumably, the Au(111) surface reconstructions may decrease the ordering of the cluster in adsorbed fullerenes, but computational description of such effects is not feasible at this moment. For the MgO substrate, calculations show the grouping of the most stable conformers near the angles of 35–40° and 75–85°, but the overall energy spread of the conformers is smaller than on metals. Although XMCD measurements are performed 2 K, it is reasonable to expect that the distribution of the conformers in the experimental samples should be different from the equilibrium for 2 K. When the sample is cooled down from room temperature, at certain point above the base temperature the angular distribution of the conformers will be frozen. Effectively, this situation can be modelled by considering conformers within a certain energy cut-off. We simulated XAS and XMCD spectra of different conformers with MULTIX code[27] (Supporting Information, Figure S8) and found that when an arbitrary energy cut-off of 50 meV is used, the simulations reproduce the experimentally found lack of the ordering on MgO|Ag-(100) and preferential in-plane alignment on Ag(100).

The PBE-D binding energy of the fullerene molecule to the surface is 2.91 eV for Au(111), 2.53 eV for Ag(100), and 1.43 eV for MgO (Table 1). The main contributions are from the dispersion interactions (E_{disp}).[25e] Deformation energy E_{def} necessary to distort the structures of the isolated $Dy_2ScN@C_{80}$ molecule and the substrate to those they adopt in the interacting system, is found to be 366 meV for Au(111), 157 meV for Ag(100), and 39 meV for MgO, to which fullerene contributions are 132, 46, and 12 meV, respectively. The remaining terms of 0.64 eV for Au(111), 0.47 eV for Ag(100), and −0.13 eV for MgO are due to the electronic contribution $E_{Coul/cov}$, which includes both Coulomb and covalent terms. Though 4–5 times smaller than dispersion, these interactions are responsible for the changes in the
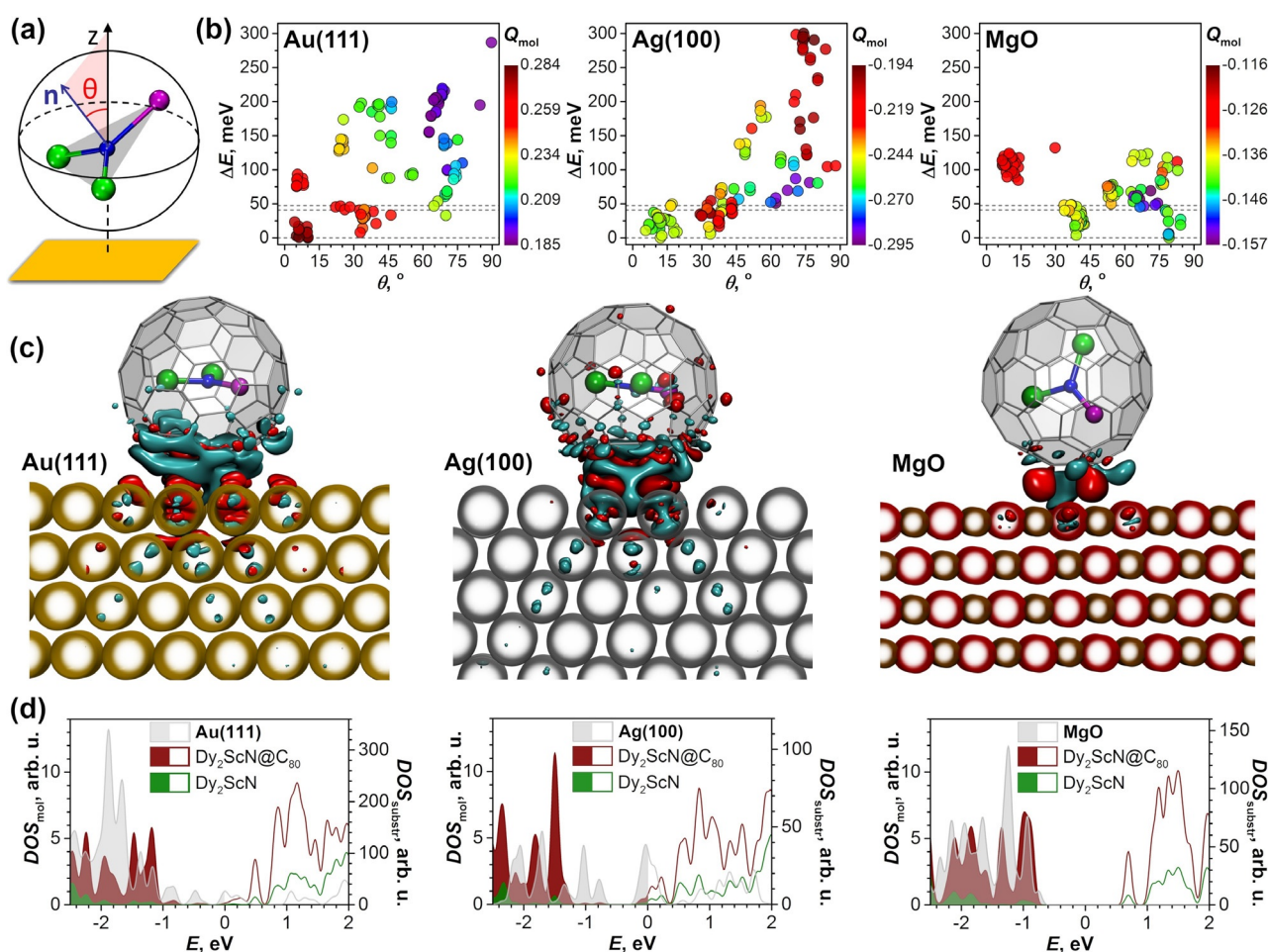
Figure 5. a) Definition of the cluster tilting angle θ as the angle between the axis z normal to the surface and the vector $\boldsymbol{n}$ radiating from the nitrogen atom perpendicular to the cluster plane; $\theta = 0°$ and $\theta = 90°$ correspond to the parallel and perpendicular alignment of the cluster versus the substrate, respectively. b) Relative energies of $Dy_2ScN@C_{80}$ conformers on Au(111), Ag(100), and MgO surfaces plotted versus θ; gray dashed lines mark the relative energies of the conformers of the free $Dy_2ScN@C_{80}$ molecule; color of the dots codes the net charge of $Dy_2ScN@C_{80}$ molecules (Q_{mol}) on a surface. c) Isosurfaces of the difference electron density for $Dy_2ScN@C_{80}$ molecule on different substrates (red color marks regions with the increased electron density, whereas cyan corresponds to the depletion of the density; all three systems are plotted at the same isovalue). d) DFT-computed density of states (DOS) near the Fermi level projected onto $Dy_2ScN@C_{80}$ molecule and Dy_2ScN cluster states (dark red and green, respectively; the axis is denoted as DOS_{mol}) and the substrate-projected DOS (DOS_{substr}, semi-transparent gray). Note that the DOS_{mol} scale is the same, whereas the DOS_{substr} scale varies in each part of the figure.

Table 1: Contributions to the fullerene-substrate binding energy [eV] and molecular and cluster charges for $Dy_2ScN@C_{80}$ adsorbed on different surfaces.

$E^{[a]}$	Au(111)	Ag(100)	MgO
E_{tot}	2.909	2.534	1.433
E_{disp}	2.634	2.223	1.603
E_{def}	−0.366	−0.157	−0.039
$E_{Coul/cov}$	0.641	0.468	−0.131
Q_{mol}	+0.28	−0.25	−0.14
$Q_{cluster}$	+3.85	+3.84	+3.85

[a] Total fullerene-substrate interaction energy E_{tot} is the energy difference between the fullerene adsorbed on the substrate and separated fullerene molecule and the substrate in their optimized structures; positive sign indicates stabilizing interaction. E_{tot} is partitioned into dispersion, deformation, and Coulomb/covalent contributions: $E_{tot} = E_{disp} + E_{def} + E_{Coul/cov}$. E_{tot}, E_{disp} and E_{def} can be computed independently, which allows estimation of $E_{Coul/cov}$.

electronic structure at the interface and hence are considered further in more details. Note also that the variation of the relative energy for different cluster orientations (Figure 5b) is mainly caused by the changes in $E_{Coul/cov}$, whereas E_{disp} remains almost identical for the whole conformer set, and variations in E_{def} are considerably smaller (Supporting Information, Table S1).

Interaction of a fullerene molecule with the substrate leads to a change in the electronic distribution of both. The net effect of this redistribution can be evaluated via the charge of the fullerene molecule (Q_{mol}) accumulated on the surface. Calculations of atomic charges with the Bader code[28] showed that $Dy_2ScN@C_{80}$ transfers $0.2–0.3\,e$ to the Au(111) substrate, but acquires a negative charge of $-(0.2–0.3)\,e$ on Ag(100) and $-(0.09–0.14)\,e$ on MgO. Importantly, despite the considerable variation of the net fullerene charge in dependence on the substrate and the cluster orientation (Figure 5b), the charge of the Dy_2ScN cluster in adsorbed molecules is

virtually the same as in the isolated $Dy_2ScN@C_{80}$ molecule and varies by less than $\pm 0.05\,e$ (compare to the $0.57\,e$ variations of Q_{mol}). The role of the Faraday cage that the fullerene plays for the endohedral cluster[7c,29] may be the reason why SMM properties of $Dy_2ScN@C_{80}$ are weakly affected by the substrate.

A closer look into the interfacial charge transfer is provided by the difference electron density $\Delta\rho$ obtained by subtraction of the electron density of separately computed $Dy_2ScN@C_{80}$ molecule and a substrate from the electron density of the whole system. Visualization of $\Delta\rho$ in Figure 5c shows that the charge redistribution is restricted to the interfacial region where the fullerene molecule contacts the substrate. The largest part of the carbon cage as well as the endohedral cluster are only weakly affected. When $Dy_2ScN@C_{80}$ is adsorbed onto the Au(111) surface, density depletion and accumulation regions are formed near the fullerene and near/at the upper gold metal atoms, respectively. For the fullerene on the Ag(100) surface, the regions of the density accumulation and depletion are intertwined in a complex manner. The spatial extension of the density affects at least two layers of Au and Ag metal atoms and small changes can be seen down to the fourth layer. For the fullerene on the MgO, the difference density has the least extended profile, and changes in the electron density are visible only in the upper layer of the substrate.

The spatial extension of $\Delta\rho$ correlates with the angular dependence of the relative energy of the $Dy_2ScN@C_{80}$ conformers. Apparently, the Dy_2ScN cluster tends to avoid the parts of the fullerene π-system interacting with the metallic surface. This can be best achieved in the parallel configuration of the Dy_2ScN cluster, in which all three metal atoms do not interact with the surface-perturbed parts of the fullerene cage. For the MgO substrate, the situation is different because the ionic substrate has strongly inhomogeneous charge distribution, and here the electrostatic interactions between the substrate and the carbon cage play an important role. As the fragments of the fullerene cage coordinated by the endohedral metals have pronounced variation of the electrostatic potential distribution,[26] the orientation of the fullerene molecule towards the substrate by such fragments may become energetically favorable.

Interactions with the substrate may also affect the electronic structure of the adsorbed fullerene. Comparison to the density of states (DOS) of the isolated $Dy_2ScN@C_{80}$ molecule (Supporting Information, Figure S12) shows that interaction with the MgO has only a minor effect on the fullerene-projected DOS. The highest-occupied states are dominated by the carbon cage, whereas the lowest-energy unoccupied states have noticeable contributions from the endohedral cluster. The LUMO of the fullerene has a distinct peak in the DOS at 0.85 eV above the Fermi level. The DFT-predicted gaps for the isolated $Dy_2ScN@C_{80}$ molecule and the molecule on the MgO are 1.65 and 1.63 eV, respectively. The interaction with the Au(111) surface results in more pronounced changes of the fullerene DOS (Figure 5d). The HOMO- and LUMO-derived peaks can be seen in the DOS at -1.09 eV and 0.59 eV, respectively. The gap between the LUMO peak and higher-energy unoccupied states is reduced

substantially. Furthermore, new states appear in the gap between the HOMO and LUMO. They originate from the hybridization with the metal bands and can be identified as surface states. Thus, the weak features inside the gap in the experimental STS spectra of $Dy_2ScN@C_{80}$ on Au(111) (Figure 2c) may have its origin here. Finally, the most pronounced changes of the DOS are found for the fullerene on Ag(100). Here the LUMO-derived feature is not a single peak anymore but is split into several components at the Fermi energy. Thus, the LUMO of $Dy_2ScN@C_{80}$ is contributing strongly to the surface states and becomes partially occupied.

Conclusion

Realization of magnetic bistability in monolayers of SMMs in contact with an electrode is a necessary step towards making use of the single-molecule nature of their magnetism in spintronic devices. In this work we showed that $Dy_2ScN@C_{80}$ fulfills this criterion. XMCD studies of the $Dy_2ScN@C_{80}$ submonolayers on Au(111), Ag(100), and MgO | Ag(100) revealed a distinctive influence of the substrates on the ordering of the endohedral cluster. On Ag(100), the Dy_2ScN units are preferentially aligned parallel to the surface, on Au(111) there is only a slight preference of the parallel alignment, whereas on MgO | Ag(100) no ordering is found at all. However, despite the strong influence of the surface on the structural ordering, the magnetic behavior of $Dy_2ScN@C_{80}$ molecules does not show a noticeable dependence on the substrate. Magnetic hysteresis with the coercivity of ca 0.4 T is found near 2 K in submonolayers of $Dy_2ScN@C_{80}$ on all three substrates. DFT calculations showed that the charge redistribution at the metal–fullerene interface is confined within the contact region. The electron transfer affects only the carbon cage, whereas the charge state of the endohedral cluster remains intact. Thus, the fullerene acts as a Faraday cage protecting the electronic and magnetic properties of the endohedral species on conducting substrates.

[1] a) D. Gatteschi, R. Sessoli, J. Villain, *Molecular Nanomagnets*, Oxford University Press, New York, **2006**; b) R. Sessoli, D. Gatteschi, A. Caneschi, M. A. Novak, *Nature* **1993**, *365*, 141–143; c) C. Benelli, D. Gatteschi, *Introduction to Molecular Magnetism*, Wiley-VCH, Weinheim, **2015**; d) D. N. Woodruff, R. E. P. Winpenny, R. A. Layfield, *Chem. Rev.* **2013**, *113*, 5110–5148.

[2] L. Bogani, W. Wernsdorfer, *Nat. Mater.* **2008**, *7*, 179–186.

[3] a) K. L. M. Harriman, D. Errulat, M. Murugesu, *Trends Chem.* **2019**, *1*, 425–439; b) J.-L. Liu, Y.-C. Chen, M.-L. Tong, *Chem. Soc. Rev.* **2018**, *47*, 2431–2453; c) Z. Zhu, M. Guo, X.-L. Li, J. Tang, *Coord. Chem. Rev.* **2019**, *378*, 350–364; d) C. A. P. Goodwin, F. Ortu, D. Reta, N. F. Chilton, D. P. Mills, *Nature* **2017**, *548*, 439–442; e) F.-S. Guo, B. M. Day, Y.-C. Chen, M.-L. Tong, A. Mansikkamäki, R. A. Layfield, *Science* **2018**, *362*, 1400–1403; f) S. T. Liddle, J. van Slageren, *Chem. Soc. Rev.* **2015**, *44*, 6655–6669.

[4] a) N. Domingo, E. Bellido, D. Ruiz-Molina, *Chem. Soc. Rev.* **2012**, *41*, 258–302; b) A. Cornia, M. Mannini, P. Sainctavit, R. Sessoli, *Chem. Soc. Rev.* **2011**, *40*, 3076–3091; c) R. J. Holmberg, M. Murugesu, *J. Mater. Chem. C* **2015**, *3*, 11986–11998; d) A. Cornia, M. Mannini in *Molecular Nanomagnets and Related Phenomena* (Ed.: S. Gao), Springer Berlin Heidelberg, Berlin, **2015**, pp. 293–330; e) J. Dreiser, *J. Phys. Condens. Matter* **2015**, *27*, 183203.

[5] a) D. Klar, A. Candini, L. Joly, S. Klyatskaya, B. Krumme, P. Ohresser, J.-P. Kappler, M. Ruben, H. Wende, *Dalton Trans.* **2014**, *43*, 10686–10689; b) L. Margheriti, D. Chiappe, M. Mannini, P. E. Car, P. Sainctavit, M.-A. Arrio, F. B. de Mongeot, J. C. Cezar, F. M. Piras, A. Magnani, E. Otero, A. Caneschi, R. Sessoli, *Adv. Mater.* **2010**, *22*, 5488–5493; c) C. Wäckerlin, F. Donati, A. Singha, R. Baltic, S. Rusponi, K. Diller, F. Patthey, M. Pivetta, Y. Lan, S. Klyatskaya, M. Ruben, H. Brune, J. Dreiser, *Adv. Mater.* **2016**, *28*, 5195–5199; d) M. Mannini, F. Bertani, C. Tudisco, L. Malavolti, L. Poggini, K. Misztal, D. Menozzi, A. Motta, E. Otero, P. Ohresser, P. Sainctavit, G. G. Condorelli, E. Dalcanale, R. Sessoli, *Nat. Commun.* **2014**, *5*, 4582; e) M. Gonidec, R. Biagi, V. Corradini, F. Moro, V. De Renzi, U. del Pennino, D. Summa, L. Muccioli, C. Zannoni, D. B. Amabilino, J. Veciana, *J. Am. Chem. Soc.* **2011**, *133*, 6603–6612; f) E. Moreno Pineda, T. Komeda, K. Katoh, M. Yamashita, M. Ruben, *Dalton Trans.* **2016**, *45*, 18417–18433; g) K. Katoh, T. Komeda, M. Yamashita, *Chem. Rec.* **2016**, *16*, 987–1016.

[6] a) M. Mannini, F. Pineider, C. Danieli, F. Totti, L. Sorace, P. Sainctavit, M. A. Arrio, E. Otero, L. Joly, J. C. Cezar, A. Cornia, R. Sessoli, *Nature* **2010**, *468*, 417–421; b) M. Mannini, F. Pineider, P. Sainctavit, C. Danieli, E. Otero, C. Sciancalepore, A. M. Talarico, M.-A. Arrio, A. Cornia, D. Gatteschi, R. Sessoli, *Nat. Mater.* **2009**, *8*, 194–197; c) L. Malavolti, V. Lanzilotto, S. Ninova, L. Poggini, I. Cimatti, B. Cortigiani, L. Margheriti, D. Chiappe, E. Otero, P. Sainctavit, F. Totti, A. Cornia, M. Mannini, R. Sessoli, *Nano Lett.* **2015**, *15*, 535–541; d) A. Cornia, M. Mannini, R. Sessoli, D. Gatteschi, *Eur. J. Inorg. Chem.* **2019**, 552–568.

[7] a) R. Westerström, A.-C. Uldry, R. Stania, J. Dreiser, C. Piamonteze, M. Muntwiler, F. Matsui, S. Rusponi, H. Brune, S. Yang, A. Popov, B. Büchner, B. Delley, T. Greber, *Phys. Rev. Lett.* **2015**, *114*, 087201; b) T. Greber, A. P. Seitsonen, A. Hemmi, J. Dreiser, R. Stania, F. Matsui, M. Muntwiler, A. A. Popov, R. Westerström, *Phys. Rev. Mater.* **2019**, *3*, 014409; c) C. H. Chen, D. S. Krylov, S. M. Avdoshenko, F. Liu, L. Spree, R. Westerström, C. Bulbucan, M. Studniarek, J. Dreiser, A. U. B. Wolter, B. Büchner, A. A. Popov, *Nanoscale* **2018**, *10*, 11287–11292.

[8] a) A. A. Popov, S. Yang, L. Dunsch, *Chem. Rev.* **2013**, *113*, 5989–6113; b) S. Yang, T. Wei, F. Jin, *Chem. Soc. Rev.* **2017**, *46*, 5005–5058.

[9] a) L. Spree, A. A. Popov, *Dalton Trans.* **2019**, *48*, 2861–2871; b) R. Westerström, J. Dreiser, C. Piamonteze, M. Muntwiler, S. Weyeneth, H. Brune, S. Rusponi, F. Nolting, A. Popov, S. Yang, L. Dunsch, T. Greber, *J. Am. Chem. Soc.* **2012**, *134*, 9840–9843.

[10] a) D. Krylov, F. Liu, A. Brandenburg, L. Spree, V. Bon, S. Kaskel, A. Wolter, B. Buchner, S. Avdoshenko, A. A. Popov, *Phys. Chem. Chem. Phys.* **2018**, *20*, 11656–11672; b) D. S. Krylov, F. Liu, S. M. Avdoshenko, L. Spree, B. Weise, A. Waske, A. U. B. Wolter, B. Büchner, A. A. Popov, *Chem. Commun.* **2017**, *53*, 7901–7904; c) C.-H. Chen, D. S. Krylov, S. M. Avdoshenko, F. Liu, L. Spree, R. Yadav, A. Alvertis, L. Hozoi, K. Nenkov, A. Kostanyan, T. Greber, A. U. B. Wolter, A. A. Popov, *Chem. Sci.* **2017**, *8*, 6451–6465; d) W. Yang, G. Velkos, F. Liu, S. M. Sudarkova, Y. Wang, J. Zhuang, H. Zhang, X. Li, X. Zhang, B. Büchner, S. M. Avdoshenko, A. A. Popov, N. Chen, *Adv. Sci.* **2019**, *6*, 1901352.

[11] a) F. Liu, G. Velkos, D. S. Krylov, L. Spree, M. Zalibera, R. Ray, N. A. Samoylova, C.-H. Chen, M. Rosenkranz, S. Schiemenz, F. Ziegs, K. Nenkov, A. Kostanyan, T. Greber, A. U. B. Wolter, M. Richter, B. Büchner, S. M. Avdoshenko, A. A. Popov, *Nat. Commun.* **2019**, *10*, 571; b) G. Velkos, D. Krylov, K. Kirkpatrick, L. Spree, V. Dubrovin, B. Büchner, S. Avdoshenko, V. Bezmelnitsyn, S. Davis, P. Faust, J. Duchamp, H. Dorn, A. A. Popov, *Angew. Chem. Int. Ed.* **2019**, *58*, 5891–5896; *Angew. Chem.* **2019**, *131*, 5951–5956; c) G. Velkos, D. S. Krylov, K. Kirkpatrick, X. Liu, L. Spree, A. U. B. Wolter, B. Buchner, H. C. Dorn, A. A. Popov, *Chem. Commun.* **2018**, *54*, 2902–2905; d) F. Liu, D. S. Krylov, L. Spree, S. M. Avdoshenko, N. A. Samoylova, M. Rosenkranz, A. Kostanyan, T. Greber, A. U. B. Wolter, B. Büchner, A. A. Popov, *Nat. Commun.* **2017**, *8*, 16098; e) F. Liu, L. Spree, D. S. Krylov, G. Velkos, S. M. Avdoshenko, A. A. Popov, *Acc. Chem. Res.* **2019**, *52*, 2981–2993.

[12] a) D. F. Leigh, C. Norenberg, D. Cattaneo, J. H. G. Owen, K. Porfyrakis, A. L. Bassi, A. Ardavan, G. A. D. Briggs, *Surf. Sci.* **2007**, *601*, 2750–2755; b) C. Nörenberg, D. F. Leigh, D. Cattaneo, K. Porfyrakis, A. L. Bassi, C. S. Casari, M. Passoni, J. H. G. Owen, G. A. D. Briggs, *J. Phys. Conf. Ser.* **2008**, *100*, 052080; c) S. Schimmel, Z. Sun, D. Baumann, D. Krylov, N. Samoylova, A. Popov, B. Büchner, C. Hess, *Beilstein J. Nanotechnol.* **2017**, *8*, 1127–1134; d) M. Treier, P. Ruffieux, R. Fasel, F. Nolting, S. Yang, L. Dunsch, T. Greber, *Phys. Rev. B* **2009**, *80*, 081403; e) T. Huang, J. Zhao, M. Feng, H. Petek, S. F. Yang, L. Dunsch, *Phys. Rev. B* **2010**, *81*, 085434.

[13] V. Vieru, L. Ungur, L. F. Chibotaru, *J. Phys. Chem. Lett.* **2013**, *4*, 3565–3569.

[14] R. Westerström, J. Dreiser, C. Piamonteze, M. Muntwiler, S. Weyeneth, K. Krämer, S.-X. Liu, S. Decurtins, A. Popov, S. Yang, L. Dunsch, T. Greber, *Phys. Rev. B* **2014**, *89*, 060406.

[15] a) E. I. Altman, R. J. Colton, *J. Vac. Sci. Technol. B* **1994**, *12*, 1906–1909; b) J. K. Gimzewski, S. Modesti, C. Gerber, R. R. Schlittler, *Chem. Phys. Lett.* **1993**, *213*, 401–406; c) J. A. Gardener, G. A. D. Briggs, M. R. Castell, *Phys. Rev. B* **2009**, *80*, 235434.

[16] a) M. Grobis, K. H. Khoo, R. Yamachika, X. H. Lu, K. Nagaoka, S. G. Louie, M. F. Crommie, H. Kato, H. Shinohara, *Phys. Rev.*

Lett. **2005**, *94*, 136802; b) T. Huang, J. Zhao, M. Feng, A. A. Popov, S. Yang, L. Dunsch, H. Petek, *Nano Lett.* **2011**, *11*, 5327 – 5332.

[17] I. Fernández-Torrente, K. J. Franke, J. I. Pascual, *J. Phys. Condens. Matter* **2008**, *20*, 184001.

[18] Á. J. Pérez-Jiménez, J. J. Palacios, E. Louis, E. SanFabián, J. A. Vergés, *ChemPhysChem* **2003**, *4*, 388 – 392.

[19] C. Piamonteze, U. Flechsig, S. Rusponi, J. Dreiser, J. Heidler, M. Schmidt, R. Wetter, M. Calvi, T. Schmidt, H. Pruchova, J. Krempasky, C. Quitmann, H. Brune, F. Nolting, *J. Synchrotron Radiat.* **2012**, *19*, 661 – 674.

[20] K. S. Pedersen, L. Ungur, M. Sigrist, A. Sundt, M. Schau-Magnussen, V. Vieru, H. Mutka, S. Rols, H. Weihe, O. Waldmann, L. F. Chibotaru, J. Bendix, J. Dreiser, *Chem. Sci.* **2014**, *5*, 1650 – 1660.

[21] a) P. Carra, B. T. Thole, M. Altarelli, X. Wang, *Phys. Rev. Lett.* **1993**, *70*, 694 – 697; b) B. T. Thole, P. Carra, F. Sette, G. van der Laan, *Phys. Rev. Lett.* **1992**, *68*, 1943 – 1946.

[22] J. Dreiser, R. Westerström, C. Piamonteze, F. Nolting, S. Rusponi, H. Brune, S. Yang, A. Popov, L. Dunsch, T. Greber, *Appl. Phys. Lett.* **2014**, *105*, 032411.

[23] M. Studniarek, C. Wäckerlin, A. Singha, R. Baltic, K. Diller, F. Donati, S. Rusponi, H. Brune, Y. Lan, S. Klyatskaya, M. Ruben, A. P. Seitsonen, J. Dreiser, *Adv. Sci.* **2019**, *6*, 1901736.

[24] a) F. D. Natterer, F. Donati, F. Patthey, H. Brune, *Phys. Rev. Lett.* **2018**, *121*, 027201; b) F. Donati, S. Rusponi, S. Stepanow, C. Wäckerlin, A. Singha, L. Persichetti, R. Baltic, K. Diller, F. Patthey, E. Fernandes, J. Dreiser, Ž. Šljivančanin, K. Kummer, C. Nistor, P. Gambardella, H. Brune, *Science* **2016**, *352*, 318 – 321.

[25] a) J. Hafner, *J. Comput. Chem.* **2008**, *29*, 2044 – 2078; b) G. Kresse, J. Hafner, *Phys. Rev. B* **1993**, *47*, 558 – 561; c) G. Kresse, D. Joubert, *Phys. Rev. B* **1999**, *59*, 1758 – 1775; d) J. P. Perdew, K. Burke, M. Ernzerhof, *Phys. Rev. Lett.* **1996**, *77*, 3865 – 3868; e) S. Grimme, *WIREs Comput. Mol. Sci.* **2011**, *1*, 211 – 228.

[26] V. Dubrovin, L.-H. Gan, B. Büchner, A. A. Popov, S. M. Avdoshenko, *Phys. Chem. Chem. Phys.* **2019**, *21*, 8197 – 8200.

[27] A. Uldry, F. Vernay, B. Delley, *Phys. Rev. B* **2012**, *85*, 125133.

[28] E. Sanville, S. D. Kenny, R. Smith, G. Henkelman, *J. Comput. Chem.* **2007**, *28*, 899 – 908.

[29] a) P. Delaney, J. C. Greer, *Appl. Phys. Lett.* **2004**, *84*, 431 – 433; b) S. M. Avdoshenko, *J. Comput. Chem.* **2018**, *39*, 1594 – 1598.